Effect of Polymerization Kinetics on Particle Morphology in Heterogeneous Systems

Martin F. Mills, Robert G. Gilbert,* and Donald H. Napper

Departments of Physical and Theoretical Chemistry, University of Sydney, Sydney, NSW 2006, Australia

Received October 2, 1989; Revised Manuscript Received February 27, 1990

ABSTRACT: The kinetics of seeded emulsion homopolymerization are modeled by formulation and solution of the reaction–diffusion equations describing the monomer and free-radical distributions within the latex particles. The simulations predict significant inhomogeneities may develop at high conversion, giving rise to core–shell morphology in the fully polymerized latex as observed experimentally. The extent of nonuniformity is most pronounced for large particles and is not present in small particles under normal conditions. The origin of inhomogeneities may be understood mechanistically in terms of the depth of penetration of free radicals into the latex particles. Dependence of the morphology on various factors including rates of diffusion, propagation, termination, entry, transfer, and exit is discussed. While predictions are in partial agreement with experimental studies of morphology, a number of uncertainties remain unresolved and warrant further investigation. However, the model provides some understanding of the role of the polymerization kinetics in determining morphology and is successful in explaining the experimentally observed lowering of the apparent propagation rate coefficient in large particles.

Introduction

The existence of intraparticle inhomogeneities in polymerizing emulsion systems has long been a subject of interest. Although core–shell and other morphologies are well established in emulsion copolymerizations, evidence for such effects in conventional emulsion homopolymerizations is less conclusive. Despite this, it is highly likely that monomer and free-radical concentration gradients do in fact occur in such systems. Such inhomogeneities could have significant effects on both the kinetics and physical properties of the system.

Early evidence suggesting the existence of intraparticle concentration gradients in emulsion homopolymerizations came from the work of Grancio and Williams,[1] who polymerized styrene "labeled" with trace amounts of butadiene onto a polystyrene seed. The latex particles obtained were sectioned, stained, and examined under the electron microscope. Results showed clear core–shell morphology, although the extent of polymer compatibility effects in these experiments remains uncertain. Further experiments using tritium as a label,[2] although qualitative in nature, appeared to support the existence of core–shell morphology. It was postulated that entropic repulsive wall or "restricted volume" effects at the surface of the monomer-swollen particle gave rise to a polymer-rich core surrounded by a monomer-rich shell and hence to core–shell morphology in the polymerized latex.[1,3]

More recently, Linné et al.,[4] Yang et al.,[5] and Fisher et al.[6] used deuterium-labeled monomer and neutron scattering to study particle morphology in seeded systems. Although the experiments and methods of analysis used by Fisher were in some respects different from those of Linné and Yang, the scattering in each case was interpreted as arising from core–shell morphology in the final product. Linné et al. concluded that the extent of inhomogeneity was dependent on the relative dimensions of the particle and the polymer chain, and this was interpreted by using the repulsive wall model of Grancio and Williams.

Kinetic evidence of nonuniformity in homopolymerizations is provided by the work of Lau et al.,[7,8] who studied the high-conversion, semicontinuous emulsion copolymerization of methyl methacrylate with small amounts of other monomers. Free-radical concentration was measured by means of ESR spectroscopy, and monomer concentration was determined by gas chromatography. Apparent propagation and termination rate coefficients obtained for two different particle sizes were found to be dependent on the particle size. These differences were attributed to the presence of nonuniform monomer and free-radical concentrations in the particles.

Chern and Poehlein[9] postulated that the surface anchoring effect of hydrophilic end groups, coupled with slow diffusion of polymer chains, could give rise to inhomogeneity and performed Monte Carlo simulations incorporating these effects. However, complete kinetic simulations using realistic rate parameters have not to date been attempted. The object of this paper is to investigate this matter theoretically by using diffusion data and kinetic models, which have only recently become available.

Theory

The present study is concerned with the role of polymerization kinetics in determining the morphology of latex particles. This is investigated by modeling the internal processes of propagation, termination, and diffusion, which occur within the latex particles, together with the external effects of interaction with the aqueous phase. A set of coupled differential equations is formulated to describe the intraparticle reaction and diffusion events occurring at high conversion while the effect of aqueous phase events is incorporated by specification of appropriate boundary conditions. Monomer and free-radical concentrations in the particles are calculated as a function of position and time, using what are termed the "pseudo-bulk" equations,[10] extended to take diffusion into account. The pseudobulk equations apply under conditions where the particles are homogeneous and the number of free radicals per particle is high (≥ 2)

$$d\bar{n}/dt = \rho - k\bar{n} - 2k_t\bar{n}^2/(N_A V_s) \quad (1)$$

$$dC_m/dt = -k_p C_m \bar{n}/(N_A V_s) \quad (2)$$

where $\bar{n}$ is the average number of free radicals per particle, ρ is the rate coefficient for entry of free radicals into latex

* Author to whom correspondence is sent.

0024-9297/90/2223-4247$02.50/0

particles, k is the rate coefficient for exit of free radicals from particles, k_t is the termination rate coefficient, C_m is the concentration of monomer in the particles, k_p is the propagation rate coefficient, N_A is Avogadro's constant, and V_s is the swollen volume of the particle.

Reaction–Diffusion Equations. We now extend eqs 1 and 2 to take spatial inhomogeneities into account. Introduction of monomer and free-radical concentrations, which are dependent on the distance r from the center of the particle, and of the Fickian diffusion expression for a spherically symmetric system leads to the set of coupled partial differential equations

$$\frac{\partial R(r,t)}{\partial t} = \frac{1}{r^2}\frac{\partial}{\partial r}\left[r^2 D_R \frac{\partial R(r,t)}{\partial r}\right] - 2k_t R(r,t)^2 \quad (3a)$$

$$\frac{\partial M(r,t)}{\partial t} = \frac{1}{r^2}\frac{\partial}{\partial r}\left[r^2 D_M \frac{\partial M(r,t)}{\partial r}\right] - k_p M(r,t) R(r,t) \quad (3b)$$

where $M(r,t)$ and $R(r,t)$ are the concentrations of monomer and free radicals, respectively, as functions of time and position in the particle, and D_M and D_R are the diffusion coefficients for monomer and free radicals, respectively. Note that the rate coefficients k_p and k_t and the diffusion coefficients D_M and D_R vary with the local monomer concentration, $M(r,t)$. Entry, exit, and other processes involving the aqueous phase are now incorporated in the boundary conditions (see later). These equations effectively model the kinetic processes occurring within a single representative particle.

A more complete treatment of this problem would be to use the Smith–Ewart equations[11] (which take compartmentalization into account) as a basis for calculations. These could be extended in much the same manner as the pseudobulk equations, albeit with some increase in computational complexity. In the analogous compartmentalized equations, $R(r,t)$ and $M(r,t)$ would be replaced by $R_i(r,t)$ and $M_i(r,t)$ (i = 0, 1, 2, ...) where the subscript i denotes particles containing i free radicals. This approach would be most appropriate for low $\bar{n}$ systems ($\bar{n} \leq 2$). Clearly the number of equations required for high $\bar{n}$ systems would soon become prohibitive.

Effect of Transfer on Kinetics. Kinetic studies[12] of the γ-initiated emulsion polymerization of styrene have shown that the relaxation process, which occurs after removal of the polymerization vessel from the γ source (effectively switching off production of new free radicals), cannot be modeled by using a single free-radical population. It was postulated that transfer events were giving rise to monomeric and oligomeric free-radical species having a relatively high mobility and hence a high termination rate. It follows that termination kinetics should take account of the chain length of the macroradicals and that transfer might also have a pronounced effect on any concentration gradients present.

Accordingly, the above equations should be extended to take into account the kinetic effects of chain length. As an example, monomeric free radicals formed by chain transfer could well undergo termination with another radical at a rate that is significantly faster than that of a large entangled macroradical. Such effects may be incorporated into the model by assuming that there are two free-radical populations present:[12] long and short. This treatment is only approximate, since in reality there would be a number of free-radical species of varying chain length and mobility. However, it is assumed that such "fine grain" effects can be ignored.[13] Given this assumption, the extension of the foregoing equations is as follows. Instead of a single free-radical species $R(r,t)$, one has the following: (1) long radicals, whose diffusion rate is given by the rigid chain limit as will be described later, and (2) relatively mobile short radicals, which are created by transfer to monomer and which may convert back into "longs" by propagation.

For most calculations, entering free radicals are treated as being long because of the surface anchoring effect of the hydrophilic end group while those that exit must be short to be reasonably soluble in the aqueous phase (see boundary conditions). The equations describing this system are

$$\frac{\partial L(r,t)}{\partial t} = \frac{1}{r^2}\frac{\partial}{\partial r}\left[r^2 D_L \frac{\partial L(r,t)}{\partial r}\right] - 2k_{tLL} L(r,t)^2 - k_{tr} L(r,t) M(r,t) - k_{tSL} S(r,t) L(r,t) + k_p S(r,t) C_m/Z \quad (4a)$$

$$\frac{\partial M(r,t)}{\partial t} = \frac{1}{r^2}\frac{\partial}{\partial r}\left[r^2 D_M \frac{\partial M(r,t)}{\partial r}\right] - k_p M(r,t)[L(r,t) + S(r,t)] \quad (4b)$$

$$\frac{\partial S(r,t)}{\partial t} = \frac{1}{r^2}\frac{\partial}{\partial r}\left[r^2 D_S \frac{\partial S(r,t)}{\partial r}\right] - 2k_{tSS} S(r,t)^2 + k_{tr} L(r,t) M(r,t) - k_{tSL} S(r,t) L(r,t) - k_p S(r,t) C_m/Z \quad (4c)$$

where $S(r,t)$ and $L(r,t)$ are the concentrations of short and long free radicals, respectively, k_{tr} is the rate coefficient for transfer to monomer, k_{tLL} is the rate coefficient for termination between two long free radicals, k_{tSL} is the short–long termination rate coefficient, k_{tSS} is the short–short termination rate coefficient, D_L and D_S are the diffusion coefficients for long and short free radicals, and Z is the chain length at which a short chain becomes a long chain.

Polymer Motion. The foregoing equations require further modification if the bulk movement of formed polymer is to be taken into account. If substantial diffusion of monomer occurs inside the latex particles, it is evident that some motion of formed polymer must also occur to compensate for localized change in monomer concentration. In addition to this, there is the overall volume contraction that takes place as monomer is converted to polymer. This is typically about 15% of the total volume for a seeded system having an initial weight fraction of polymer (W_p) of 0.5. Two approaches are adopted to include these effects. The first of these involves inclusion of polymer diffusion into the kinetic scheme as follows:

To maintain mass balance in each volume element, the rate of gain or loss of polymer must be equal and opposite to the rate of change of monomer; i.e.

$$\frac{\partial M(r,t)}{\partial t} = -\frac{1}{M_W}\frac{\partial P(r,t)}{\partial t} \quad (5a)$$

and so from eq 3b we have

$$\frac{1}{M_W}\frac{\partial P(r,t)}{\partial t} = -\frac{1}{r^2}\frac{\partial}{\partial r}\left[r^2 D_M \frac{\partial M}{\partial r}\right] + k_p MR \quad (5b)$$

where M_W is the monomer molecular weight and $P(r,t)$ is the concentration of polymer in units of mass per unit volume. Volume contraction is not accounted for by this method and it is assumed that the densities of monomer and polymer are the same (this deficiency will be removed later). Note that it is not necessary to know explicitly the diffusion coefficient for the polymer itself.

While the above equation describes the overall polymer migration caused by monomer diffusion, it is necessary to distinguish between "old" polymer, originating from the seed, and "new" polymer, formed subsequently in order to resolve the morphology of the particle. This is achieved

by assuming (as is physically reasonable for a homopolymerization) that the gain or loss of new or old polymer by diffusion is proportional to its local weight fraction. That is, if there is more of one polymer type present, then there is proportionately more of this material to be displaced:

$$\frac{1}{M_W}\frac{\partial P_{old}(r,t)}{\partial t} = -\frac{1}{r^2}\frac{\partial}{\partial r}\left[r^2 D_M \frac{\partial M}{\partial r}\right]\left[\frac{P_{old}}{P_{old}+P_{new}}\right] \quad (5c)$$

$$\frac{1}{M_W}\frac{\partial P_{new}(r,t)}{\partial t} = -\frac{1}{r^2}\frac{\partial}{\partial r}\left[r^2 D_M \frac{\partial M}{\partial r}\right]\left[\frac{P_{new}}{P_{old}+P_{new}}\right] + k_p MR \quad (5d)$$

Note that the equation for new polymer also has a gain term due to propagation.

An alternative treatment of the problem of polymer displacement ensures that uniform density is approximately maintained as follows: The simulation is stopped at regular intervals and the size of each volume element is corrected for gain or loss of monomer by diffusion and for volume change due to polymerization. The simulation is then restarted by using the corrected volume elements and the process repeated until final conversion is reached. The advantage of this method is that it correctly reproduces the volume contraction of the particle as monomer is converted to polymer. For this reason it would be particularly suited to the modeling of continuous systems (as distinct from batch systems) where large volume changes may occur. On the negative side, it is found that the time taken for computation is considerably increased. Both methods described to calculate the effect of polymer motion have been implemented and results are found to be consistent given the approximations involved. This confirms that both approaches are in fact more or less equivalent and that the effect of volume contraction, ignored in eq 5, is indeed unimportant with regard to inhomogeneity in the systems considered here.

Repulsive wall effects have been ignored for the present. Such effects could be included as a potential term in the reaction–diffusion equations (converting them to Smoluchowski equations) if a functional form for the potential were known. However, the relative importance of repulsive wall effects are at present uncertain and will be discussed in detail in a separate paper.[14]

Boundary Conditions. The solution of the reaction–diffusion equations requires the specification of the boundary conditions both at the center and at the surface of the particle. For $r = 0$, this is given simply by the requirement that the derivatives be well-behaved:

$$\left[\frac{\partial R(r,t)}{\partial r}\right]_{r=0} = 0 \qquad \left[\frac{\partial M(r,t)}{\partial r}\right]_{r=0} = 0 \quad (6)$$

At the particle surface, on the other hand, the boundary conditions essentially describe how the particle interacts with the aqueous phase. Since free radicals and monomer behave differently, they are treated separately in the following discussion.

Boundary Conditions for Free Radicals. When a water soluble initiator is used, free radicals are produced in the aqueous phase and subsequently undergo entry into the particles. The flux into the particles may be obtained from the entry rate coefficient, ρ. For the system of eqs 3a and 3b, by Fick's first law

$$\text{flux per unit area} = \left[D_R \frac{\partial R(r,t)}{\partial r}\right]_{r=R_s} = \frac{\rho}{4\pi R_s^2} \quad (7a)$$

where R_s is the swollen radius of the particle. Exit has been neglected in eq 7a, which will be valid for most systems considered since (1) the exit rate is likely to be small, in particular for large particles at high conversion, and (2) the probability of aqueous phase termination before a reentry event occurs is usually exceedingly small[15] so there will be no observable effect on the kinetics.

The model can be extended to show the effect of exit as follows. It is generally accepted that exit occurs by diffusion out of the particle of a short free radical created by transfer. In the limit of maximum possible exit rate, all monomeric or short free radicals that diffuse to the surface of the particle will exit and terminate in the aqueous phase. In this case, the following boundary conditions apply for the system of eq 4:

$$[S(r,t)]_{r=R_s} = 0 \quad (7b)$$

$$\left[D_L \frac{\partial L(r,t)}{\partial r}\right]_{r=R_s} = \frac{\rho}{4\pi R_s^2} \quad (7c)$$

Calculations will be reported for both limits: systems obeying eq 7a (negligible exit) and those obeying eq 7b (maximum possible rate of exit).

Boundary Conditions for Monomer. For a continuous or interval II batch emulsion polymerization there is a more or less constant flux of monomer into the latex particles. However, for batch polymerization in interval III, a small and steadily decreasing amount of monomer is present in the aqueous phase and so the monomer flux decreases with increasing conversion. This is significant for monomers that are less insoluble in the aqueous phase. For MMA at a W_p of 0.8 and a typical particle number concentration ($N_c = 10^{15}$–10^{17} dm^{-3}), aqueous phase monomer amounts to less than 10% of the total monomer in the system. To a first approximation, therefore, monomer in the aqueous phase can be neglected, resulting in zero flux of monomer at the surface:

$$\left[\frac{\partial M(r,t)}{\partial r}\right]_{r=R_s} = 0 \quad (7d)$$

A first-order correction for aqueous monomer was incorporated in some calculations by using mass balance to calculate the amount of monomer remaining in the aqueous phase and the partition relation[10]

$$[M]_{aq} = [M]_{aq,sat}\left[\frac{C_m}{C_{m,sat}}\right]^n \quad (8)$$

to obtain monomer concentration at the surface of the particle at thermodynamic equilibrium. The subscripts aq and sat refer to aqueous and saturation concentrations, respectively. The exponent n will depend on the monomer under consideration. This method does not fully describe the dynamic nature of monomer exchange, but given the observed effect, further refinement is not warranted.

Initial Conditions. Prior to commencement of the simulation, it is necessary to specify the initial distribution of monomer and free radicals in the system. The choice of initial conversion will depend on the precise conditions being modeled. In general, the initial monomer and free-radical distributions are made uniform so that any concentration gradients that arise are due solely to the kinetic processes being modeled. Results are found to be

insensitive to the precise choice of initial conditions provided the initial W_p is not too high.

Rate Parameters. Solution of eqs 3a and 3b above requires knowledge of the rate parameters k_t and k_p and of the diffusion coefficients D_M and D_R. Recent theoretical developments provide the basis for determining these parameters as a function of polymer weight fraction.

In the high-conversion regime, when reactions are likely to become diffusion controlled, it is appropriate to express the propagation rate coefficient in the manner[16]

$$k_p = \left[\frac{1}{k_{p,d}} + \frac{1}{k_p^\circ}\right]^{-1} \tag{9a}$$

where k_p° and $k_{p,d}$ are the chemical and diffusion-limited rate coefficients, respectively. The diffusive term is given by the Smoluchowski equation for diffusion-controlled bimolecular reaction[17]

$$k_{p,d} = 4\pi(D_M + D_R)(R_M + R_R) \tag{9b}$$

where R_M and R_R are the radii of interaction of monomer and free radicals, respectively. Both R_M and R_R may be approximated by $\sigma/2$, where σ is the Lennard-Jones diameter of the monomer.[17] Given experimental $k_p(W_p)$ and the rate of free-radical diffusion (see below), it is therefore possible to find $D_M(W_p)$ and, conversely, to estimate k_p from D_M.

The macroradical diffusion coefficient is sensitive to both the conversion and the size of the free radical. In the "rigid chain limit" where translational motion of polymer chains is assumed to be completely frozen, the reactive chain end can move only by propagation. This is termed "reaction diffusion",[17] and the diffusion rate coefficient for this process may be calculated from the propagation rate

$$D_L = D_R = k_p C_m a^2/6 \tag{10}$$

where a is the root-mean-square end-to-end distance of the polymer chain per square root of the number of monomer units. Solution of the evolution equations (eq 4) using the formulation of eq 10 incorporates completely the surface anchoring effects in the Monte Carlo simulations of Chern and Poehlein.[9]

If the free radical is a "short" or oligomeric species, center-of-mass diffusion must be added to the reaction-diffusion term:[12]

$$D_S = k_p C_m a^2/6 + \frac{D_M}{Z}\sum_{j=1}^{Z}\frac{1}{j} \tag{11}$$

The second term in this expression assumes first that there is a steady-state population of free radicals and second that the rate of center-of-mass diffusion is inversely proportional to chain length.[12] To calculate the termination rate coefficients, the appropriate diffusion coefficients are substituted into the Smoluchowski expression.[12] Thus for long–long termination

$$\begin{aligned} k_t = k_{tLL} &= 2\pi N_A(D_L + D_L)\sigma \\ &= 2\pi N_A a^2 C_m k_p \sigma/3 \end{aligned} \tag{12}$$

Note that eq 12 differs by a factor of 2 from that originally presented.[17,18] This corrects an error in the original work.

From the diffusion above it can be seen that the rate parameters are closely interrelated, and, in fact, estimates for all rate parameters in the rigid chain limit may be obtained if the value of any one of them is known.

Parameter Values. Values of the rate parameters used in the simulations were taken from representative experimental data at a temperature of 50 °C. Although

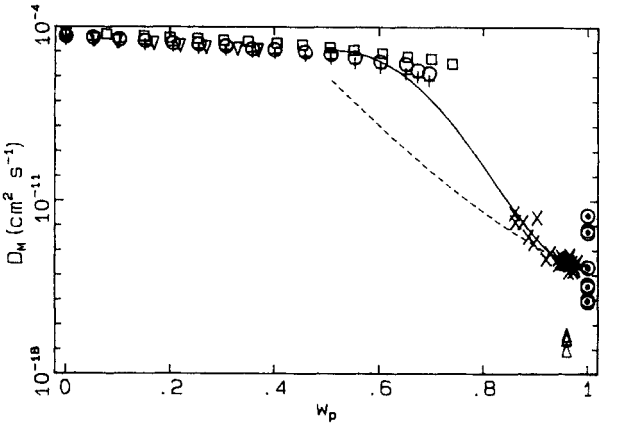

Figure 1. Diffusion coefficients of small penetrants in PMMA around 50 °C: (△) TIWS,[30] 45–60 °C; (⊙) organic vapors,[31] 50 °C; (▽) MMA,[32] 50 °C; (+) benzene,[33] 40 °C; (○) benzene,[33] 60 °C; (□) acetone,[33] 40 °C; (x) MMA,[19] 50 °C. Broken line is the least-squares fit to kinetic data. Unbroken line is the least-squares fit to kinetic data and data of Kosfeld and Schlegel[33] (benzene, 40 °C).

the equations presented thus far may in principle be applied to any appropriate monomer system, the simulations presented herein are mainly for the homopolymerization of MMA. This is primarily because experimental values for the requisite rate parameters are available over the range of conversion of interest. Furthermore, these data are in accord with the assumptions of the previous section.

Experimental values for the propagation rate coefficient for MMA have been obtained at high conversion using a combination of ESR and dilatometric techniques.[16] After breakdown as in eq 9a into diffusion and chemical contributions, the following fit to the experimental data was obtained[13]

$$k_{p,d} = k_p^\circ \exp[X_1(W_p - X_2)] \tag{13}$$

where $X_1 = -41.5$ and $X_2 = 0.87$ (note that this fit corrects a small error in the fit presented in the original work).[16] This W_p dependence was used to derive "kinetic" values for D_m by rearrangement of eqs 9a and 9b. A recent compilation from the literature of direct experimental diffusion data for various tracers (obtained by using various techniques including forced Rayleigh scattering) shows acceptable agreement with the "kinetic" diffusion coefficients[13] (Figure 1) for tracers similar to the monomer unit. A similar literature compilation of diffusion coefficients is also available for styrene.[18] Values for the termination rate coefficient calcualted by using eq 12 are also in agreement with experimental estimates[19] at high conversion where the polymer becomes glassy and hence the rigid chain limit becomes appropriate.

For use in the present calculations, a convenient functional form for the dependence of D_M on monomer concentration was obtained by least-squares fitting to the kinetically derived diffusion coefficients (see dashed line in Figure 1). Note that there are no kinetic data for D_M at conversions less than 80% (although data for tracer molecules are available) but that the fit is unimportant here as D_M is not rate determining (see eq 9a and Figure 1). Calculations using a more general fit, including some tracer data (solid line in Figure 1), showed no significant difference in final morphology. The remaining rate parameters (D_R, k_p, and k_t) are obtained through eqs 10–12.

Those parameters that are independent of conversion are given for MMA and styrene in Table I. Note that the

Table I
Constants Used in Simulation

	MMA	styrene
k_p°, dm^3 mol^{-1} s^{-1}	580	258
a, nm	0.585	0.602
σ, nm	0.69	0.74
k_{tr}, dm^3 mol^{-1} s^{-1}	0.033	0.0093
$C_{m,sat}$, mol dm^{-3}	6.6	5.8
$[M]_{aq,sat}$, mol dm^{-3}	0.15	0.0043
Z	50	50
n	0.60	1.67

Table II
Entry Rate Coefficients for MMA[a]

run	P°, g	M°, g	[I], mol dm^{-3}	V_{total}, cm^3	ρ, 10^{-3} s^{-1}
R93	1.769	9.46	0.0142	126	378
R94	1.924	9.46	0.0069	126	150
R82	1.801	9.53	0.0047	126	100
R83	1.794	9.50	0.0024	126	52
R86	1.869	9.45	0.0006	126	14

[a] P° is total initial polymer mass. M° is total initial monomer mass. V_{total} is the total polymerization volume. [I] is the initiator concentration. The N_c of this system is about 7×10^{16} dm^{-3}.

k_{tr} value is for transfer to monomer. This value is readily adjusted if one is simulating experiments incorporating a chain-transfer agent. The value given for Z corresponds to the entanglement spacing of the polymer chains.[17] This is the length at which the growing free radical is virtually immobilized by interactions with neighboring chains.

While the parameter values considered thus far are essentially independent of events in the aqueous phase, the value of the entry rate coefficient, ρ, may depend strongly on the particle size, the particle number concentration N_c, and the initiator concentration. Table II shows experimental estimates of ρ for varying concentrations of persulfate initiator.[10] These results were for an interval II seeded polymerization of MMA having a final solids content of about 10% and a seed particle radius of 46 nm. A value of 0.08 s^{-1} is adopted as being representative for a 50-nm particle at typical initiator concentrations (1–2% by weight of monomer) and a solids content of 20% by weight. Note that this value is subject to some uncertainty as there is considerable scatter in the experimental data.

To obtain equivalent values of ρ for different particle sizes (identical initiator concentration and latex solids content), a new model for entry[20] is used, which predicts that ρ is proportional to $1/N_c$. The model, which is mathematically similar to the HUFT model for homogeneous nucleation, is based on the assumption that entry is controlled by aqueous phase events, these being decomposition of initiator, aqueous phase propagation to a critical degree of polymerization z whereupon entry occurs, and termination. Consideration of these competing processes leads to the expression

$$\rho = \frac{2k_d[I]}{N_c}\left[\frac{(2k_d[I]k_{t,aq})^{0.5}}{k_{p,aq}[M]_{aq}} + 1\right]^{1-z} \quad (14)$$

where k_d is the rate coefficient for initiator dissociation, [I] is the initiator concentration, and $k_{t,aq}$ and $k_{p,aq}$ are the aqueous termination and propagation rate coefficients, respectively. Calculations of the entry rate using this model are in agreement with a range of experimental data including the effect of initiator concentration, ionic strength, surfactant coverage, and temperature for styrene, MMA, and butyl acrylate.

For PMMA, the first term in square brackets in eq 14 is small, so ρ is relatively invariant with conversion and the entry rate may be held constant in the simulations. Experimental results for polystyrene over W_p values ranging from 0.5 to 0.7 indicate that ρ is not strongly dependent on W_p although the scatter in the data is such that no definite conclusion may be made in this regard.[20] It is noted that if any dropoff in initiator efficiency with conversion does occur, it is more likely to be at high conversion where $[M]_{aq}$ decreases more rapidly.

Numerical Solution. Calculations were performed by using a software package provided by the Numerical Algorithms Group Library for solution of nonlinear parabolic partial differential equations. The technique combines the use of the Gear algorithm[21] with the finite difference method in a fourth-order integration of the equations.

Results

Representative results for small and large PMMA particles, having radii of 25 and 250 nm, are shown in parts a–d of Figure 2. Monomer and free-radical concentrations are given as a function of distance r from the center of the particle for polymer weight fractions ranging from 0.8 to 0.99. Transfer (short–long termination) and exit have been ignored in these calculations unless stated otherwise.

It is found that, for the 25-nm particle, no significant inhomogeneities arise until nearly 99% conversion, whereas for the 250-nm particle, inhomogeneities first become apparent at a W_p of 0.9 and increase dramatically at high conversion. In the latter instance it is found that most free radicals remain near the surface, this being a result of radical flux from outside the particles combined with limited diffusion inside the particles. Thus, entering radicals do not penetrate as effectively into the larger particles at high conversion. Qualitatively similar predictions have been made previously by Chern and Poehlein[9] on the basis of Monte Carlo simulations of the free-radical distribution in nonuniform latex particles. Their simulations were based on the assumption that entering free radicals are anchored to the surface by their hydrophilic end groups. This assumption is implicit in the present study when the rigid chain limit is used because diffusion of the active free-radical site is by propagation only.

The high surface concentration of free radicals noted in Figure 2b is found to lead to depletion of monomer near the particle surface (Figure 2d), a result which is in conflict with the repulsive wall model first proposed by Keusch et al.[3] on the basis of experimental investigation of particle morphology. They postulated that the polymerizing latex particles comprise a polymer-rich core surrounded by a monomer-rich shell and that monomer polymerizes in situ to give the observed core–shell morphology. It was argued that repulsive wall effects at the particle–water interface tend to push polymer chains away from the surface. In other words, conformational freedom is restricted near the surface and so entropic considerations favor higher polymer density near the core.

While the kinetic picture of the polymerization process provided by the present study is quite different from the repulsive wall model of Grancio and Williams, it is found that the morphology of the resulting latex particles is qualitatively the same in both instances. If the conversion per unit volume obtained in the present study is integrated to give the spatial distribution of newly formed polymer at complete conversion, it is evident (Figure 3) that proportionately more conversion has occurred near the surface. Inclusion of polymer diffusion into the scheme (Figure 4) shows that old polymer, and to a lesser extent

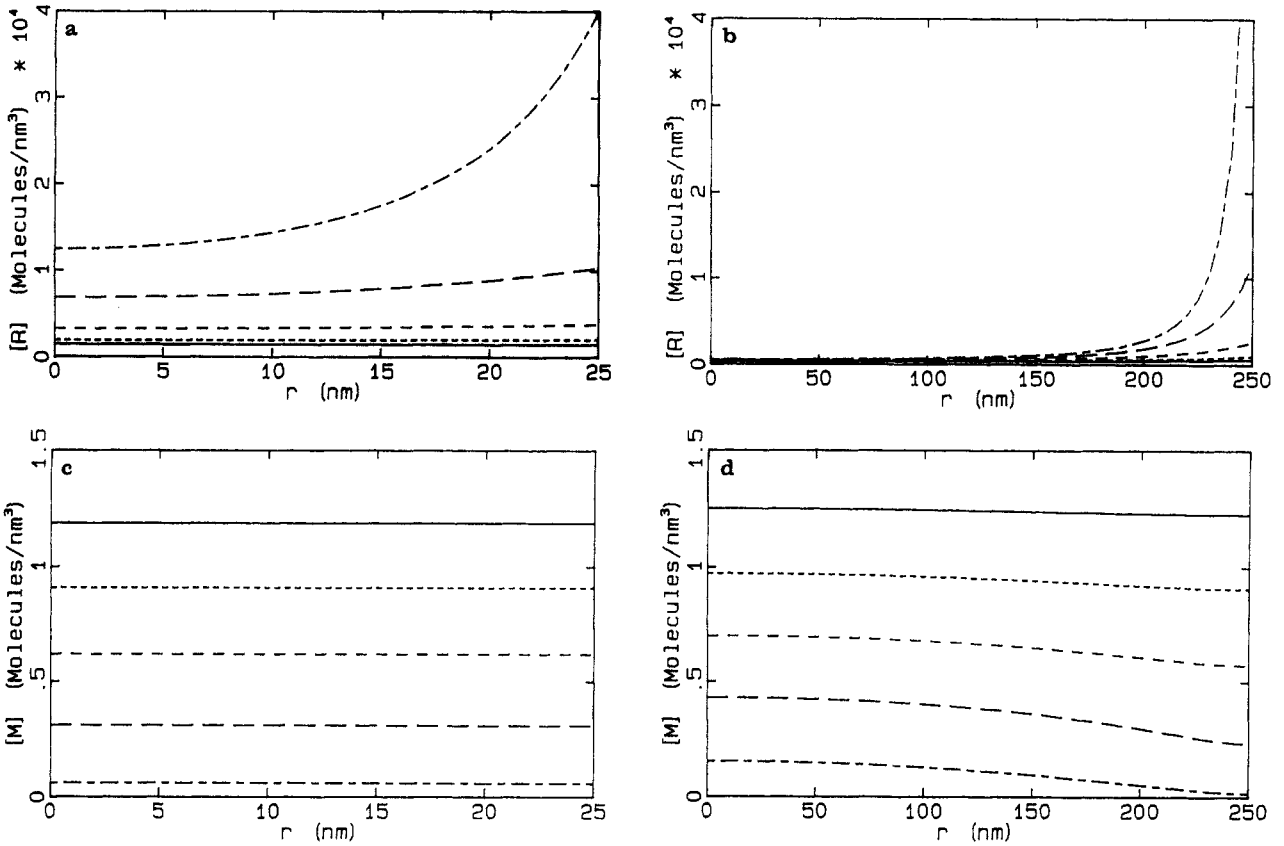

Figure 2. (a) Computed free-radical concentration as a function of distance from center of particle at polymer weight fractions of 0.8–0.99 (R_s = 25 nm, ρ = 0.02 s^{-1}, W_p^* = 0.5): (—) W_p = 0.80; (· · ·) W_p = 0.85; (- - -) W_p = 0.90; (– –) W_p = 0.95; (– · –) W_p = 0.99. (b) Computed free-radical concentration as a function of distance from center of particle at polymer weight fractions of 0.8–0.99 (R_s = 250 nm, ρ = 2 s^{-1}, W_p^* = 0.5). Curves as for Figure 2a. (c) Computed monomer concentration as a function of distance from center of particle at polymer weight fractions of 0.8–0.99 (R_s = 25 nm, ρ = 0.02 s^{-1}, W_p^* = 0.5). Curves as for Figure 2a. (d) Computed monomer concentration as a function of distance from center of particle at polymer weight fractions of 0.8–0.99 (R_s = 250 nm, ρ = 2 s^{-1}, W_p^* = 0.5). Curves as for Figure 2a.

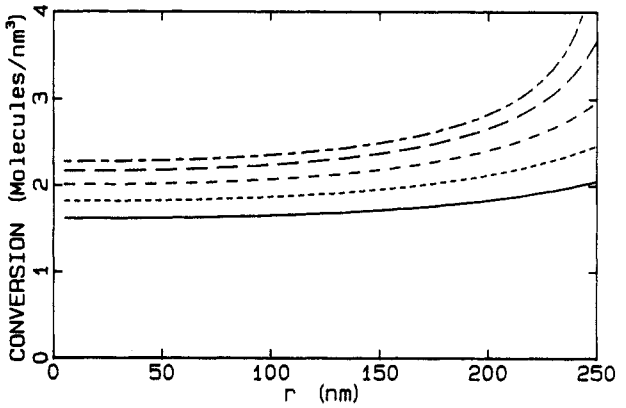

Figure 3. Total conversion of monomer as a function of distance from center of particle at polymer weight fractions of 0.8–0.99 (R_s = 250 nm, ρ = 2 s^{-1}, W_p^* = 0.5). Curves as for Figure 2a.

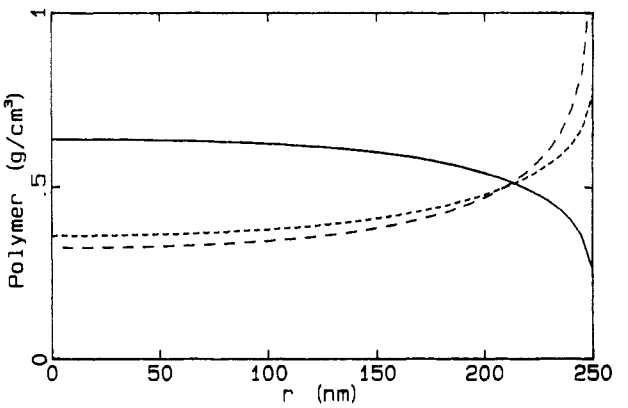

Figure 4. Total conversion and concentration of new and old polymer as a function of distance from center of particle at a W_p of 0.99 (W_p^* = 0.5, ρ = 20 s^{-1}, R_s = 250 nm): (—) P_{old}; (· · ·) P_{new}; (- - -) total conversion.

new polymer, is displaced toward the core as polymerization proceeds.

A convenient measure of core–shell morphology for comparative purposes is provided by $X_{1/2}$, a quantity that we define as the percent conversion of second-stage monomer outside the unswollen radius of the seed (or "half-volume" at a W_p of 0.5). A result of $X_{1/2}$ = 100% would be obtained for a particle that showed complete core–shell morphology. The value of $X_{1/2}$ (Table III, run A) obtained for a swollen radius of 25 nm is 50%, indicating that new polymer is uniformly mixed with old, whereas for a 250-nm radius (run B), $X_{1/2}$ is significantly greater (approximately 60%) in the shell.

The percent conversion (or $X_{1/2}$) and other quantities such as the effective k_p (see below) may also be used to estimate the significance of parameters other than particle size. The results of a series of such calculations are given in Table III. These we now discuss in turn.

(1) Computational results show that the evolution of the system is fairly insensitive to the initial conditions such as W_p^* (the initial W_p) and the initial distribution of monomer and free radicals (runs B and D).

(2) As expected, correction for monomer in the aqueous phase (run F) also has a relatively small effect. The flux of monomer results in a slight increase in $X_{1/2}$. This effect

Table III
Effect of Various Parameters on Morphology[a]

run	radius, nm	W_p^*	W_p	ρ, s^{-1}	$k_p(W_p)$, $dm^3\ mol^{-1}\ s^{-1}$	$k_{p,eff}$, $dm^3\ mol^{-1}\ s^{-1}$	$X_{1/2}$
				MMA			
A	25	0.5	0.99	0.02	6.8	6.8	50
B	250	0.5	0.99	2	6.8	2.5	60
C	250	0.8	0.96	2	15	11	59
D	250	0.8	0.99	2	6.8	2.7	62
E	250	0.5	0.99	20	6.8	0.5	64
F	250	0.8	0.96	2	15	13	60
				Styrene			
G	250	0.5	0.99	0.8	3.8	2.7	55
H	250	0.5	0.99	20	3.8	0.4	70
				Parameters Varied			
I	250	0.5	0.98	20	0.85	0.02	64
J	250	0.5	0.99	20	6.8	1.2	77
K	250	0.5	0.99	20	6.8	0.3	74
L	25	0.5	0.99	20	6.8	2.5	60
				Transfer Included			
M	250	0.8	0.99	2	6.8	2.7	64
N	250	0.8	0.99	2	6.8	3.3	64
O	250	0.8	0.99	2	6.8	3.8	63
P	250	0.8	0.99	2	6.8	3.8	61
				Exit Included			
Q	250	0.5	0.99	2	6.7	4.1	61
R	250	0.5	0.99	2	6.7	6.6	75
S	250	0.5	0.99	2	6.7	3.4	59
T	250	0.5	0.99	2	6.7	6.7	64

[a] W_p^* is initial conversion. $k_p(W_p)$ is the value of k_p as a function of W_p given by eqs 9a and 9b. $k_{p,eff}$ is the effective k_p given by eq 15. Descriptions of runs are as follows: F, includes aqueous monomer (eq 8); G, polystyrene with short–long termination and entry of shorts; H, polystyrene; I, D_M divided by 10 (This also changes dependent variables D_R, k_t, and k_p through eqs 9–12.); J, k_t multiplied by 10; K, D_R and k_t divided by 10; L, high entry rate (small particle); M, $k_{tr} = 0.033\ dm^3\ mol^{-1}\ s^{-1}$, entry of shorts; N, $k_{tr} = 0.33\ dm^3\ mol^{-1}\ s^{-1}$, entry of shorts; O, $k_{tr} = 3.3\ dm^3\ mol^{-1}\ s^{-1}$, entry of shorts; P, $k_{tr} = 3.3\ dm^3\ mol^{-1}\ s^{-1}$, entry of longs; Q, $k_{tr} = 0.033\ dm^3\ mol^{-1}\ s^{-1}$, $Z = 50$; R, $k_{tr} = 3.3\ dm^3\ mol^{-1}\ s^{-1}$, $Z = 50$; S, $k_{tr} = 0.033\ dm^3\ mol^{-1}\ s^{-1}$, $Z = 1$; T, $k_{tr} = 3.3\ dm^3\ mol^{-1}\ s^{-1}$, $Z = 1$.

might be expected to be greatly enhanced in continuous systems.

(3) An at first surprising result was that inclusion of transfer (without exit) has virtually no effect on the morphology. The reason for this becomes apparent on examination of the diffusion coefficients used in the simulation. Over a W_p range of 0.8–1.0, it was found that the value of D_M was of the order of 2–10 times the value of D_R. Therefore, short free radicals would not have a sufficiently high relative mobility to have a large effect on the overall free-radical distribution. Note that it is assumed here that polymer chain length has no effect on D_M, as is likely to be the case if the polymer molecular weight is high.[22] Comparison of runs D, O, and P confirms that inclusion of short and long free-radical species has had little overall effect.

(4) The increase in transfer rate that occurs on addition of chain-transfer agent may be crudely estimated by variation of the rate coefficient for transfer to monomer (runs M–O). Only at very high transfer rates is any effect observed, and even then, the changes are small.

(5) If exit is included as per eq 7b, a quite dramatic increase in $X_{1/2}$ is seen with increasing k_{tr} (runs Q–T). The short free-radical distribution for run R is given in Figure 5. These results may be understood as follows. If a free radical immediately exits after transfer, then the effective penetration of the growing free radical into the particle is determined simply by the length to which the chain

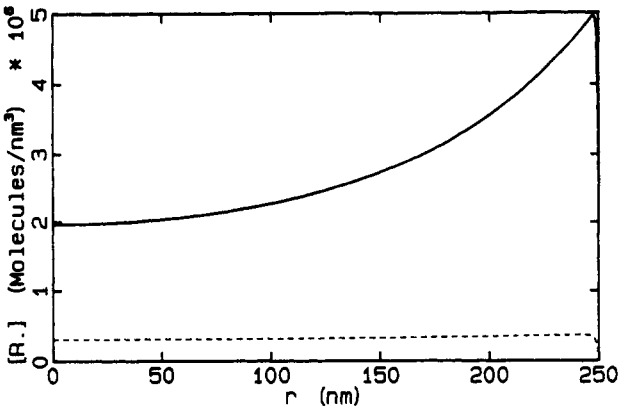

Figure 5. Concentration of short free radicals as a function of radial distance for run R: (···) $W_p = 0.90$; (—) $W_p = 0.99$.

grows before transfer. If, on the other hand, no exit occurs, then the free radical continues to propagate inward. Note that inhomogeneity increases with Z as this increases the population of free radicals that may exit. This suggests that the most important factor in determining morphology (in the absence of transfer) is the control of polymer chain dimensions relative to that of the particle exerted by the rate parameters. If most chains grow to a length that is somewhat smaller than the particle radius, then most new growth will occur near the surface. Most inhomogeneity is obtained at high W_p because the length of the polymer chains becomes smaller due to decrease in k_p.

(6) Some calculations have been performed for styrene (runs G and H), although it is noted that only limited experimental data are available for the high-conversion rate parameters in this system. Overall, the results are qualitatively similar to those obtained for MMA, although for a given ρ, the value of $X_{1/2}$ is somewhat higher. This reflects the slightly different values of the rate parameters for the two systems.

In order to better understand the effect of the rate parameters on the particle morphology, the values of individual parameters were varied arbitrarily in some simulations, although it is stressed here that no direct physical significance should be attached to these values. Results are given in runs I–L in Table III.

(7) From these results, it is apparent that the extent of core–shell morphology is more strongly dependent on the relative rates of free-radical diffusion, propagation, and termination than on their absolute values. Thus more core–shell character will arise if the rate of termination is high relative to the rate of free-radical diffusion (as is seen for run J), whereas if all rate coefficients are varied in the same manner (runs I and K), the effect on morphology is reduced. These results are consistent with the conclusions from exit calculations.

(8) Similar considerations to the above apply to the effect of the entry rate on morphology. Increasing ρ results in a significant increase in inhomogeneity (compare runs B and E) since the concentration of free radicals near the particle surface is enhanced. It is important therefore that the correct entry model and entry rate coefficient be used in calculations. Note that it is possible to produce core–shell morphology in a 25-nm particle (run L) if a sufficiently high (perhaps achievable by use of redox initiator) value of ρ is used.

It was stated earlier that core–shell morphology observed experimentally is qualitatively in agreement with results of the present study. While this is true in a broad sense, closer examination shows that there remains a number of

unresolved discrepancies as will now be discussed in more detail.

Staining Results. Grancio and Williams[1,2] reported core–shell morphology in polystyrene particles ranging in size from 25- to 300-nm radius, with apparently complete separation of core and shell in most instances. Simulations using the present model for a single monomer–polymer system wherein monomer and polymer are mutually soluble do not appear capable (at least for physically reasonable variation of parameters) of producing significant core–shell morphology in particles as small as 25 nm nor, for that matter, complete core–shell morphology in particles of any size. These apparent discrepancies may be explained if the experimental results arise at least in part from incompatibility of butadiene and styrene (see Introduction), and/or their respective polymers, or if repulsive wall effects are important. Note also that there is some uncertainty in the experimental determination of the spatial extent of staining.

Keusch and Williams[2] also performed experiments using oil-soluble initiator in place of the usual water-soluble initiator. Results indicated that core–shell morphology was still present, although it was somewhat reduced in extent. It was originally suggested that this result could not be produced kinetically because free radicals generated at random inside the particles could not give rise to concentration gradients. However, they were unable to explain the observed reduction in core–shell morphology when compared with a water-soluble initiator. In fact (if one ignores for the time being the unresolved differences regarding the extent of core–shell morphology), the results may be explained kinetically as follows: An initiator that is only soluble in the organic phase should show reduced efficiency at high conversion, as it does in bulk polymerizations because of geminate recombination.[23] Since the initiator used by Grancio and Williams (benzoyl peroxide) is water soluble to some extent, the major locus of initiation at high conversion (when core–shell morphology is most likely to arise) may become the aqueous phase. Hence, the origin of the inhomogeneity could be the same as that for the water-soluble initiator. Inhomogeneity would be reduced by residual free-radical production inside the particles.

SANS Results. Recent SANS experiments by Fisher et al.[5] looked at the structure of latex particles produced by swelling a PMMA seed with deuterated MMA and polymerizing. The seed latex had a particle radius of about 50 nm, and second-stage polymerization was commenced at a W_p of around 0.85. Scattering intensity was analyzed by using a concentric sphere model corrected for particle size polydispersity effects. It is noted that latices were quite monodisperse and that no blank subtraction was used in this analysis. Results were consistent with the presence of core–shell morphology, the radius of the core corresponding to that of the original seed. However, small differences between the fit and the experimental curve may have been due to some interpenetration of core and shell.

This system was modeled in the present study although it is noted that experimental data were for a redox system polymerized at a temperature of 90 °C. Since the entry rate coefficient for the redox system used is unknown (although it is expected to be very high), simulation results are presented for two different entry rates: one slightly higher than that expected for a persulfate system and the other several orders of magnitude higher (Figure 6). It is unclear whether the resolution of the SANS technique used is sufficient to differentiate between more complete core–shell morphology and profiles of the type shown in Figure 6 and whether the use of an even higher value for ρ is warranted.

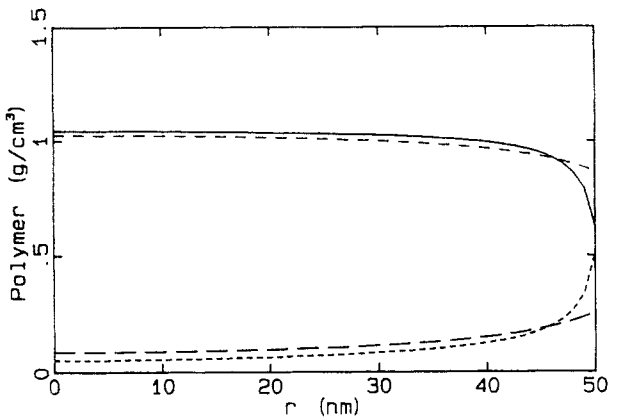

Figure 6. Simulation of the experiment of Fisher et al.[4] (W_p^* = 0.85, final W_p = 0.99, R_s = 50 nm): (—) P_{old} (ρ = 20 s^{-1}); (···) P_{new} (ρ = 20 s^{-1}); (- - -) P_{old} (ρ = 2000 s^{-1}); (– –) P_{new} (ρ = 2000 s^{-1}).

Detailed SANS investigation of particle morphology for a range of particle sizes and molecular weights has been carried out for styrene homopolymerizations by Linné et al.[4] and Yang et al.[5] The latices examined had average radii ranging from 15 to 150 nm. It is noted, however, that the particle size distributions were highly polydisperse (Linné et al., Figure 1 and Table II). Isotopic labeling was used together with blank subtraction and contrast matching techniques to remove unwanted information from the scattering data, with the objective of leaving only information about the polymer chain conformations and any core–shell morphology present. Fitting of the Debye random-coil model to the scattering data used the radius of gyration of the polymer chains as an adjustable parameter. The molecular weight thus obtained was compared to GPC results, with the ratio M_w(SANS)/M_w(GPC) being taken to be a measure of the core–shell morphology present. It was claimed that the anomalously large values obtained for M_w(SANS) in some instances were a result of the labeled core scattering as a single "supermolecular" entity. It is noted that the fit to scattering data was very poor where significant departures from M_w(GPC) were observed.

This analysis indicated the presence of inhomogeneities that were greater than those predicted by the present study, both in extent and in particle size range. The results were interpreted as showing morphology that could vary from core–shell to uniform for any particle size, depending on relative dimensions of the particles and the polymer molecules. Maximum segregation of core and shell polymer was reported when the ratio of the molecular weight to the square of the particle diameter was about 0.1. These results were attributed to repulsive wall effects, with the relative chain dimensions being the main factor determining the strength of the perturbation caused by the interface.

In order to understand better the underlying mechanisms involved, further experiments were carried out examining the swollen seed rather than the final polymerized product.[24] Similar trends with molecular weight were observed, but it was also found that segregation of monomer and polymer decreased with increased conversion. These results add further weight to the proposed repulsive wall mechanism. However, separate SANS experiments on swollen latices by Ottewill[25] indicated that swelling by monomer was uniform. Unfortunately, there are no molecular weight data available for the experiments of Ottewill at present.

In attempting to reconcile the data of Linné et al. with the present study, it is noted that control of molecular weight was achieved experimentally by addition of CCl_4 as chain-transfer agent. It is possible therefore that transfer itself might be having some influence on morphology. However, kinetic simulations show little if any dependence on transfer even for high values of k_{tr} and hence on molecular weight unless exit or increased termination is involved. Experimentally, it is observed that entry and exit rates may vary considerably[26] on addition of CCl_4 and so it is possible that some such effect is taking place. A number of other factors also need to be considered, and these are discussed below:

(1) Repulsive wall effects have not been considered in the present study and may need to be included in addition to kinetic effects. If so, they may well constitute the major factor determining particle morphology. This question will be the subject of a separate paper.[14]

(2) The particle size distributions of the latices used in the SANS experiments of refs 4 and 5 appear to have been very broad. This may have led to artifacts in the interpretation of scattering results. One possible source of error is the blank subtraction, which is crucial to the analysis.

(3) Scattering intensity was analyzed by using the Debye random-coil model.[27] Departures from ideality were taken to be a measure of "supermolecular" structure in the particles. This analysis does not address in a rigorous way the poorness of the fit. Note that this approach is quite different from that used by Fisher et al. and Ottewill.

(4) Isotope effects may lead to phase separation of deuterated and protonated polymers. Wignall and Bates[28] discussed in some detail the applicability of isotopic labeling to polymer systems and found that anomalously high SANS-determined molecular weights may be a manifestation of the slight thermodynamic differences between the polymers. This is most likely for high molecular weights and high concentrations of labeled polymer such as are present here. Note, however, that isotope effects should not be significant for any experiments on swollen latices.

Effects on Kinetics. Insight into the relationship between the kinetics and the morphology of the system may be gained by closer examination of the rate coefficients k_p and k_t. Lau et al.[7] used ESR[16,29] and gas chromatography to measure the average free-radical and monomer concentrations in a semicontinuous system and hence, from the overall rate, deduced a value of k_p via the rate equation:

$$R_p = \frac{-d[M]_{av}}{dt} = k_p[M]_{av}[R^\bullet]_{av} \qquad (15)$$

The use of eq 15 does not take inhomogeneities into account, and the sensitivity of this assumption can be treated by using the computer-generated "data" of the present study as follows: An equivalent or "effective" k_p is calculated by first integrating over the volume of the particle to obtain averaged values for $M(r,t)$, $R(r,t)$, and the total rate of polymerization, R_p, and then by substituting these into eq 15. Calculated and experimental results are given in Table IV. It should be noted first that there are a number of important differences between the experimental and model systems:

(1) Calculated values are for homopolymerization of MMA while the experimental results were for the copolymerization of MMA–butyl acrylate–methacrylic acid (91:8:1). The copolymer system could not be modeled because the extra rate parameters are unknown.

Table IV
Comparison of Calculated and Experimental k_p[a]

radius, nm	W_p	$k_p(W_p)$, dm^3 mol^{-1} s^{-1}	$k_{p,eff}$,[6] dm^3 mol^{-1} s^{-1}	calcd ρ, s^{-1}	calcd $k_{p,eff}$, dm^3 mol^{-1} s^{-1}
25	0.95	19		0.02	19
	0.97	11	170	0.02	11
250	0.90	75		0.2	74
				2	73
				20	50
	0.95	19	35	0.2	16
				2	13
				20	7
	0.97	11		0.2	10
				2	8
				20	3

[a] $k_p(W_p)$ is the value of k_p as a function of W_p given by eqs 9a and 9b. $k_{p,eff}$ is the effective, or average, k_p as determined from eq 15.

(2) Calculations are for a batch system whereas the experimental results were for a semicontinuous reactor. This means that the experimental system was held at essentially constant W_p.

(3) Redox initiator was used in the experiments. The entry rate is therefore unknown although it is certain to be high.

(4) Experimental data reported for different particle sizes were not at the same W_p.

In the light of these differences, full comparison of experimental and calculated results is not possible.

Despite the above qualifications, it appears (Table IV) that the conclusion that the experimentally observed lowering of the measured k_p in the larger particle is due to concentration gradients is borne out at least qualitatively by the present study. It is important to remember here that the extent of k_p lowering will be strongly dependent on the concentration and type of initiator used. However, it is interesting to note (Table III) that the extent of k_p lowering is not necessarily a reflection of the final morphology.

Westmoreland et al.[7] also used ESR to estimate average values of k_t for different particle sizes. Entry was switched off by ceasing addition of redox initiator, and the resulting free-radical decay was recorded. This was then fitted to a second-order rate law to obtain k_t:

$$\frac{d[R^\bullet]}{dt} = -2k_t[R^\bullet]^2 \qquad (16)$$

We can examine the validity of this procedure by comparison with our simulated data as was done for k_p. It was found that the simulated time dependence of $[R^\bullet]$ could not be fitted to a second-order rate law (Figure 7). This is not surprising if one notes that k_t is steadily decreasing due to increasing conversion during the decay period and that any inhomogeneity present may introduce even greater nonlinearity. A second-order fit to the simulation data could only be obtained if k_t were independent of W_p for the duration of the relaxation. This discrepancy is unresolved at present, although it is noted that the ESR technique is subject to some uncertainty.

Effective k_t values obtained from simulations using the same procedure as was used for the effective k_p show two opposing effects (Table V). This is apparent from inspection of $k_{t,eff}$ at various stages of conversion. Nonuniformity in free-radical concentration at relatively low conversions is seen to result in an increase in $k_{t,eff}$. This is simply because termination is faster if the free radicals are close to each other. On the other hand, for the same run at high conversion, where there is also nonunifor-

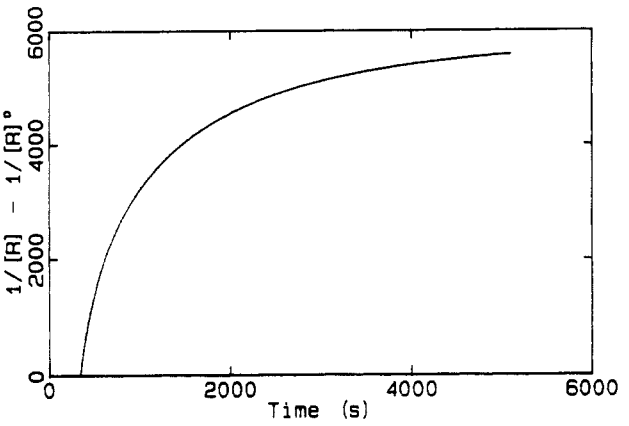

Figure 7. Computed plot of free-radical decay after switching off entry. $[R]^\bullet$ is the free-radical concentration at the start of the relaxation. If decay is second order, a linear plot should be obtained (ρ = 2 s^{-1}, $W_p^\bullet$ = 0.8, R_s = 250 nm).

Table V
Calculated Effective k_t[a]

run	radius, nm	$W_p^\bullet$	W_p	ρ, s^{-1}	$k_t(W_p)$, $dm^3\ mol^{-1}\ s^{-1}$	$k_{t,eff}$, $dm^3\ mol^{-1}\ s^{-1}$
A	25	0.5	0.99	0.02	0.24	0.23
B	250	0.5	0.99	2	0.24	0.24
E	250	0.5	0.80	20	270	297
			0.99		0.24	0.091
H	250	0.5	0.80	20	204	239
			0.99		0.14	0.10
I	250	0.5	0.99	20	0.06	0.01

[a] $k_t(W_p)$ is the value of k_t as a function of W_p given by eq 12. $k_{t,eff}$ is the effective k_t. Runs as for Table III.

mity in monomer, the effective termination rate coefficient is lowered due to lowering of the diffusion coefficients. The value of $k_{t,eff}$ is even more strongly reduced when the diffusion coefficient in monomer is arbitrarily lowered, resulting in a less uniform monomer distribution.

Conclusions

In summary, computer modeling of emulsion polymerizations in the diffusion-limited regime has shown that significant spatial inhomogeneities may arise particularly in large particles at high conversion. When persulfate initiator is used, particles remain homogeneous to a good approximation at lower conversion and for smaller particles even at quite high conversions. These results are of fundamental importance in that they support the general validity of conclusions drawn from kinetic experiments where homogeneity has been assumed[10-13,16-20] (usually low conversion and small particle size). Moreover, the presence of inhomogeneity for large particles at high conversion is of interest from an industrial viewpoint since most polymerization is carried out in this regime. In this regard, kinetic simulations appear successful in predicting the experimentally observed lowering of k_p in large latex particles at high conversion and may assist in interpreting similar experiments to determine k_t.

The nonuniformities observed in the simulations are found to give rise to core–shell morphology in the final product as has been observed experimentally. The extent of core–shell morphology produced appears to depend primarily on the effective penetration range of the entering free radical and hence on the combination of factors such as conversion, particle size, and initiator concentration. Thus simulations have enabled determination of the underlying mechanisms that give rise to nonuniformity. These results may be of assistance in understanding the origin of core–shell morphology in other systems such as dispersion and suspension polymerizations and copolymer systems, although in the latter case, compatibility effects will usually tend to dominate.

Although results so far are encouraging, there remain some discrepancies between theory and experiment, which have not yet been fully resolved and warrant further theoretical and experimental investigation. There are some doubts about the validity of many of the experiments, and, in addition, it is difficult in many instances to model the experimental conditions because appropriate rate coefficients are at present unknown. It has yet to be established to what extent kinetic and thermodynamic effects may both contribute to the morphology of latex particles formed in emulsion homopolymerizations.

Acknowledgment. The financial support of the Australian Research Grant Scheme is gratefully acknowledged. We also thank Prof. L. H. Sperling and Prof. A. Klein for sending us preprints of refs 4, 5, and 24 and W. Lau, D. G. Westmoreland, and R. W. Novak for sending us preprints of refs 7 and 8. Thanks are also due to members of the Sydney University Polymer Group for many helpful discussions and suggestions.

References and Notes

(1) Grancio, M. R.; Williams, D. J. *J. Polym. Sci., Part A-1* **1970**, *8*, 2617.
(2) Keusch, P.; Williams, D. J. *J. Polym. Sci., Polym. Chem. Ed.* **1973**, *11*, 143.
(3) Keusch, P., Graff, R. A.; Williams, D. J. *Macromolecules* **1978**, *7*, 304.
(4) Linné, M. A.; Klein, A.; Sperling, L. H.; Wignall, G. D. *J. Macromol. Sci., Phys.* **1988**, *B27* (2 & 3), 181.
(5) Yang, S. I.; Klein, A.; Sperling, L. H. *J. Polym. Sci., Polym. Phys. Ed.* **1989**, *27*, 1649.
(6) Fisher, L. W.; Melpolder, S. M.; O'Reilly, J. M.; Ramakrishnan, V.; Wignall, G. D. *J. Colloid Interface Sci.* **1988**, *123*, 24.
(7) Lau, W.; Westmoreland, W.; Novak, R. W. *Macromolecules* **1987**, *20*, 457.
(8) Westmoreland, D. G.; Lau, W. *Macromolecules* **1989**, *22*, 496.
(9) Chern, C. S.; Poehlein, G. W. *J. Polym. Sci., Polym. Chem. Ed.* **1987**, *25*, 617.
(10) Ballard, M. J.; Napper, D. H.; Gilbert, R. G. *J. Polym. Sci., Polym. Chem. Ed.* **1984**, *22*, 3225.
(11) Smith, W. V.; Ewart, R. H. *J. Chem. Phys.* **1948**, *16*, 592.
(12) Adams, M. E.; Russell, G. T.; Casey, B. S.; Gilbert, R. G.; Napper, D. H.; Sangster, D. F. *Macromolecules*, in press.
(13) Russell, G. T.; Napper, D. H.; Gilbert, R. G., to be published.
(14) Croxton, C. A.; Mills, M. F.; Gilbert, R. G.; Napper, D. H., to be published.
(15) Maxwell, I. A., to be published.
(16) Ballard, M. J.; Gilbert, R. G.; Napper, D. H.; Pomery, P. J.; O'Sullivan, P. W.; O'Donnell, J. H. *Macromolecules* **1986**, *19*, 1303.
(17) Russell, G. T.; Napper, D. H.; Gilbert, R. G. *Macromolecules* **1988**, *21*, 2133.
(18) Casey, B. S.; Maxwell, I. A.; Morrison, B. R.; Gilbert, R. G. *Makromol. Chem., Macromol. Symp.* **1990**, *31*, 1.
(19) Ballard, M. J.; Sangster, D. F.; Napper, D. H.; Gilbert, R. G. *J. Polym. Sci., Polym. Chem. Ed.* **1986**, *24*, 1027.
(20) Maxwell, I. A.; Morrison, B. R.; Gilbert, R. G.; Napper, D. H. *Macromolecules*, in press.
(21) Gear, G. W. *Numerical Initial Boundary Problems in Ordinary Differential Equations*; Prentice-Hall: New York, 1971.
(22) Yu, D. H. S.; Torkelson, J. M. *Macromolecules* **1988**, *21*, 1033.
(23) Russell, G. T.; Napper, D. H.; Gilbert, R. G. *Macromolecules* **1988**, *21*, 2141.
(24) Yang, S. I.; Klein, A.; Sperling, L. H., submitted for publication in *Macromolecules*.
(25) Ottewill, R. H. *Future Directions in Polymer Colloids*; El-Aasser, M. S., Fitch, R. M., Eds.; Martinus Nijhoff: Dordrecht, The Netherlands, 1987.
(26) Lichti, G.; Sangster, D. F.; Whang, B. C. Y.; Napper, D. H.; Gilbert, R. G. *J. Chem. Soc., Faraday Trans. 1* **1982**, *78*, 2129.
(27) Debye, P. *J. Phys. Colloid Chem.* **1947**, *51*, 18.
(28) Wignall, G. D.; Bates, F. S. *Makromol. Chem., Macromol. Symp.* **1988**, *15*, 105.

(29) Ballard, M. J.; Gilbert, R. G.; Napper, D. H.; Pomery, P. J.; O'Donnell, J. H. *Macromolecules* **1984**, *17*, 504.
(30) Leest, Y.; Smets, G. *J. Polym. Sci., Polym. Chem.* **1988**, *26*, 913.
(31) Berens, A. R.; Hopfenberg, H. B. *J. Membr. Sci.* **1982**, *20*, 283.
(32) Callaghan, P., private communication.
(33) Kosfeld, R.; Schlegel, J. *Angew. Makromol. Chem.* **1973**, *29/30*, 105.

Registry No. PMMA, 9011-14-7; MMA, 80-62-6; styrene, 100-42-5; polystyrene, 9003-53-6.